Redox Reactions of the Non-Heme Iron in Photosystem II: An EPR Spectroscopic Study[†]

James P. McEvoy[‡] and Gary W. Brudvig*

Department of Chemistry, Yale University, P.O. Box 208107, New Haven, Connecticut 06520-8107

Received July 24, 2008; Revised Manuscript Received October 8, 2008

ABSTRACT: Photosystem II (PSII) contains a non-heme ferrous ion, located on the stromal side of the protein in close proximity to quinones A and B (Q_A and Q_B). We used EPR spectroscopy to examine the temperature-dependent redox reactions of the iron-quinone site, using it as a probe of potentially physiologically relevant proton-coupled electron-transfer (PCET) reactions. Complete chemical oxidation of the non-heme iron at ambient temperatures was followed by cryogenic photoreduction, producing a temperature-dependent yield of $Fe^{2+}Q_A$ (or $Fe^{3+}Q_A^-$)$\cdots$$Chl^+/Car^+/Y_D^\bullet$ charge separations. These charge separations were subsequently observed to partially recombine in the dark at cryogenic temperatures. We observed no double photochemical charge separations upon illumination at temperatures $\leq$30 K, demonstrating that Q_A and Fe^{3+} together act as a single electron-accepting moiety at very low temperatures. Our results indicate the existence of two populations of the iron-quinone site in PSII, one whose Fe^{3+} signal is abolished by illumination at liquid helium temperatures and one whose Fe^{3+} signal is abolished by illumination only above 75 K. The observation of non-heme iron photoreduction at cryogenic temperatures (possibly at liquid helium temperatures and certainly above 75 K) implies the existence of a low reorganization energy proton-transfer (ET) pathway within the protein to the non-heme iron environment, of possible relevance to the PCET reactions of Q_B and/or the non-heme iron itself. Furthermore, we observed the partial reoxidation of the non-heme iron by charge recombination with previously oxidized chlorophyll, carotenoid, and Y_D within PSII. This electron transfer might be important in the photoprotective transfer of oxidative power away from P_{680}^+ and the oxygen-evolving complex in stressed PSII centers.

Photosystem II (PSII)[1] is a membrane-intrinsic, multisubunit protein found in green plants and cyanobacteria that catalyzes the oxidation of water to dioxygen. Electrons are transferred from the photooxidized chlorophyll center P_{680} via pheophytin to quinone Q_A and move from there to their final destination in PSII, quinone Q_B. Both of these quinones lie on the stromal side of the membrane. After Q_B has accepted two electrons from Q_A and two protons from the chloroplast stroma, being reduced first to the semiquinone and then to the quinol (Q_BH_2) redox state, it diffuses from its binding pocket into the membrane, carrying its electrons and protons to the cytochrome b_6f complex and continuing the linear electron-transfer (ET) pathway of oxygenic photosynthesis. P_{680}^+, meanwhile, oxidizes (via a redox-active tyrosine residue, tyrosine Z of the D1 subunit) the manganese-containing oxygen-evolving complex (OEC) which lies on the lumenal side of PSII. The OEC catalyzes the oxidation of water to dioxygen by progressing through a series of oxidation states known as S-states.

Besides these "primary" redox cofactors involved in the main-chain electron-transfer pathway, PSII also contains a number of "secondary" redox cofactors. At sufficiently low temperatures, the OEC cannot advance in S-state, and the secondary cofactors act as alternative electron donors to P_{680}^+ under illumination. These donors include tyrosine Z (*1*), tyrosine D (the D2 subunit analogue of tyrosine Z) (*2*), cytochrome b_{559} (*3*), and a variety of chlorophyll and carotenoid molecules. Chlorophyll and carotenoid photooxidation at cryogenic temperatures has been extensively characterized in this laboratory and elsewhere (*4*−*6*) with EPR, near-IR and Raman spectroscopy, and has been recently reviewed (*7*). These redox reactions have been implicated in physiological photoprotection mechanisms, whereby redox-active chlorophylls and carotenoids are oxidized under high-light conditions and subsequently nonphotochemically quenched to avoid oxidative damage to the reaction center (*3, 7*).

A non-heme ferrous ion lies between Q_A and Q_B in PSII. The metal's presence on the acceptor side of the enzyme was demonstrated by electron paramagnetic resonance (EPR) spectroscopy, the non-heme Fe^{2+} interacting magnetically with Q_A^- to give a broad signal in the $g = 1.6-1.9$ region

[†] This work was supported by a grant from the DOE, Office of Basic Energy Sciences, Division of Chemical Sciences, DE-FG02-05ER15646. NSF Grant CHE-0215926 provided funds to purchase the ELEXSYS E500 EPR spectrometer.

* Corresponding author. Tel: 203-432-5202. Fax: 203-432-6144. E-mail: gary.brudvig@yale.edu.

[‡] Current address: Department of Chemistry, Regis University, 3333 Regis Blvd., Denver, CO 80221-1099.

[1] Abbreviations: au, arbitrary units; Car, carotenoid; Chl, chlorophyll; EPR, electron paramagnetic resonance; ET, electron transfer; OEC, oxygen-evolving complex; P_{680}, primary electron donor; PCET, proton-coupled electron transfer; PSII, photosystem II; Q_A, primary quinone electron acceptor; Q_B, secondary quinone electron acceptor; Y_D, tyrosine D (D2-Y160); Y_Z, tyrosine Z (D1-Y161).

10.1021/bi8013888 CCC: $40.75
Published on Web 11/17/2008

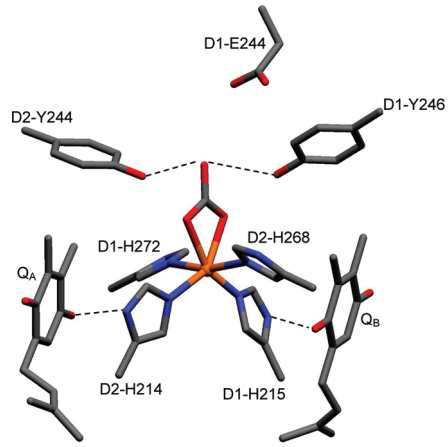

FIGURE 1: Coordination of the non-heme iron in PSII according to the 3.0 Å resolution crystal structure of Loll et al. (*19*), Protein Data Bank accession number 2AXT. Amino acid residues are shown as side chains only, and the quinones have been truncated at C-15. D1-Y246 and D2-Y244 appear to hydrogen bond to the bicarbonate (<4 Å away), interactions represented by dashed lines (NB hydrogen atoms not shown), while D1-E244 is also very close (<4 Å). D2-K264, which is not shown, is a little more distant (>4 Å) from the bicarbonate, although this residue was suggested to hydrogen bond to the bicarbonate in an earlier structure (*18*).

(*8*). The Fe^{2+} ion was later shown by Petrouleas and Diner (*9*) to be identical to the previously discovered "Q_{400}" acceptor in PSII (*10*). The redox-coupled proton transfer implied by a pH-dependent reduction potential has recently been observed electrometrically (*11*). The proton in the reduced state is believed to reside on an amino acid residue(s) near to the iron, which displays an apparent pK_a of >8 in the ferrous state and 5.3 in the ferric state (*12*). The non-heme iron may be oxidized both photochemically and by chemical oxidants such as ferricyanide, although the latter method has been found to give higher yields of Fe^{3+} (*13*). Photochemical reduction of the preoxidized non-heme Fe^{3+} is observed if ET from Q_A to Q_B is prevented, either by the binding of an inhibitor in the Q_B site (*10*) or by the use of low temperatures (*14*). The preoxidized non-heme Fe^{3+} has previously been used as an electron acceptor in PSII at moderately low temperatures, illuminations between 200 and 240 K having been used to produce double oxidation of the OEC ($S_1 \rightarrow S_2 \rightarrow S_3$), and the accumulated S_3 state then characterized by X-ray absorption spectroscopy (*14*) as well as by EPR spectroscopy (*15, 16*). The non-heme Fe^{3+} has been characterized by EPR spectroscopy (*9*), displaying peaks at $g \approx 8$ and $g \approx 5.6$. These signals have been shown to arise from the ground-state and first excited-state Kramers' doublets of high-spin Fe^{3+}, respectively (*13, 17*).

Recent crystallographic studies of PSII (*18, 19*) have confirmed that the non-heme iron is coordinated by four histidines (two from the D1 subunit and two from the D2 subunit) and by a single chelating bicarbonate anion (see Figure 1). The ion is ca. 7 Å away from both Q_A and Q_B, and two of its ligating histidines form parts of the two quinone binding pockets: D1-His215 in the case of Q_B and D2-His214 in the case of Q_A. The presence of bicarbonate as a ligand, which was originally suggested on the basis of sequence comparison with the bacterial reaction center (*20*), was confirmed by examining its competition with NO as a ligand to the iron (*21*) and later studied with Fourier-transform infrared (FTIR) spectroscopy (*22*). FTIR spectroscopy has indicated that the bicarbonate ion switches from a chelating to a monodentate binding mode when the iron is oxidized (*22*). Besides NO, bicarbonate has been substituted by a variety of carboxylate ligands (*23, 24*), with varying effects on the iron's reduction potential. Since little correlation was found between the pK_a of the exogenous carboxylate ligands and the redox properties of the iron (*24*), it is unlikely that the protonation state of the exogenous ligand is tightly coupled to the charge on the non-heme iron. Recent calculations have suggested that the pH dependence of the non-heme iron's reduction potential is due, in part, to the changing protonation state of the conserved D1-E244 residue, although all of the nearby titratable residues appear to play a role (*25*).

The physiological function of the non-heme iron in PSII remains unclear. Its depletion (*26*) leads to minimal change in the environment of Q_A (*27*) and a modest 20−30% increase in the rate of electron transfer from pheophytin to Q_A (*28*). However, electron transfer from Q_A to Q_B is abolished in PSII from which the non-heme iron has been removed (*28*). The non-heme iron apparently plays an important role in PSII's quinone redox chemistry, although its high reduction potential (relative to the quinones) makes it unlikely to be physiologically redox-active. Various experiments have shown that the metal is functionally associated with both quinone-binding sites in PSII (*29, 30*), and the non-heme iron has been specifically implicated in the control of proton transfer at and around Q_B (*31*). Because the cyanide-substituted center demonstrates unchanged electron-transfer kinetics between Q_A and Q_B (*32*), it seems that the bicarbonate ligand is not directly involved in these protonation reactions, although it might exert an electrostatic effect on other species (*25*). The metal center has also been hypothesized to be involved in oxygen redox chemistry, perhaps as a superoxide dismutase (*33, 34*).

In the present work, we have chemically preoxidized the non-heme iron of PSII in order to use the $Fe^{3+}Q_A$ site as (1) a cryogenic electron acceptor in charge separations involving chlorophyll and carotenoid secondary electron donors and (2) a probe of proton-coupled electron transfer at the non-heme iron itself. We achieved complete oxidation of the non-heme iron by substituting its exogenous bicarbonate ligand by glycolate ($CH_2(OH)CO_2^-$), reducing the reduction potential of the center to +340 mV (*24*). We have examined the cryogenic temperature dependence of the photoreduction of the preoxidized non-heme iron, demonstrating that low temperatures "freeze in" two conformations of the $Fe^{3+}Q_A$ center which differ in their EPR response to illumination. At temperatures ≤30 K, illumination abolished the Fe^{3+} EPR signal in 70−75% of the centers, whereas the signal was retained in the remaining 25−30%. Significant double charge separation to produce $Fe^{2+}Q_A^-$ was not observed, leading us to conclude that, at these temperatures, the $Fe^{3+}Q_A$ site acts as a single electron acceptor. At 143 K, illumination totally abolished the Fe^{3+} signal in the remaining iron-quinone centers and produced a $Fe^{2+}Q_A^-$ signal, showing that both the non-heme iron and Q_A were able to accept electrons at these higher temperatures. We compared the use of $Fe^{3+}Q_A$ and $Fe^{2+}Q_A$ as the majority electron acceptor at 30 K, examining the accompanying photooxidation of chlorophylls, carotenoids, and tyrosine D, and concluded that the yields and stability of oxidized products are the same in

each case, confirming that the $Fe^{3+}Q_A$ site acts as a single electron-accepting moiety at this temperature. In PSII in which the non-heme iron was fully preoxidized, partial charge recombination of Chl^+, Car^+, and $Y_D^\bullet$ with the cryogenically photoreduced iron-quinone center was observed at low temperatures. A preliminary report of these findings has been published (*35*).

MATERIALS AND METHODS

PSII-enriched (BBY) membranes were isolated from fresh market spinach (*36*). Dim green LED light was used throughout the procedure. The membranes were finally resuspended in a buffer containing 0.4 M sucrose, 15 mM NaCl, and 20 mM MES, adjusted to pH 6.5 with concentrated NaOH at 0 °C. The oxygen-evolving activities of the membranes were assayed at 25 °C with a YSI Model 5300 Clark electrode under saturating red light using ferricyanide and 2,5-dichlorobenzoquinone (DCBQ, twice recrystallized from ethanol) as electron acceptors and ranged from 300 to 500 μmol of O_2 (mg of chl)$^{-1}$ h^{-1}. Prior to the EPR experiments, sodium glycolate and potassium ferricyanide (both from Sigma Aldrich) were added to the PSII membrane sample to give respectively 40 and 4 mM final concentrations, and the sample was incubated overnight on ice in darkness. Ferricyanide was washed out as required by washing three times (with ca. 10 sample volumes in total) in resuspension buffer plus 40 mM sodium glycolate, under very dim green LED light. The chlorophyll concentration of the final EPR sample was ca. 2.5 mg of chl mL^{-1}, measured according to the method of Arnon (*37*). Dioxygen was removed from the surface of the EPR sample by purging with helium gas for 5 min at 198 K. Persistent dioxygen EPR signals were removed as required with three cycles of a freeze−pump−thaw procedure (also using helium gas at 198 K) previously described by Boussac and co-workers (*38*). EPR spectroscopy was performed at X-band on a Bruker Biospin Elexsys E500 spectrometer, using a Super High Sensitivity cavity. Temperature control was achieved with an Oxford ESR900 liquid helium cryostat and an Oxford ITC4 temperature controller. Illumination of the sample within the EPR cavity was performed with a 150 W halogen lamp, using a 6 cm long water filter to remove infrared radiation. A Newport Oriel liquid light guide was used to carry light into the cavity. Illuminations outside the cavity were performed with a 100 W halogen lamp. Temperatures of 77, 198, and 273 K were achieved with appropriate baths in an insulated and internally reflective glass dewar. Other low temperatures outside the cavity were achieved using a home-built cooled N_2(g) flow system and measured with a digital temperature sensor (Omega Engineering). Stoichiometric oxidation of Y_D was accomplished after the addition to the PSII membrane sample of 1 μL of 100 mM phenyl-1,4-benzoquinone (PPBQ) (Sigma Aldrich, twice recrystallized from ethanol) in DMSO, to a final concentration of 500 μM. The sample was then illuminated at 273 K for 1 min, incubated for 10 s in the dark at the same temperature, frozen to 77 K, and quickly scanned (*39*). These stoichiometric $Y_D^\bullet$ signals were subsequently used for quantitation of both the $g \approx 2$ signals ($Y_D^\bullet$ and Chl^+/Car^+) and the Fe^{3+} signal, according to the method of Aasa et al. (*17, 40*). Since the Fe^{3+} and $Y_D^\bullet$ signals were obtained under different conditions, the double integral of the stoichiometric $Y_D^\bullet$ signal was corrected according to these differences in microwave power, modulation amplitude, and temperature. Equation 1 was then used to obtain the percentage quantitation for Fe^{3+}:

$$\%\ Fe^{3+} = 100 \times \frac{x}{6.78 \times 10^{-4}} \times \frac{2}{y} \times z \qquad (1)$$

where x = integral of Fe^{3+} signal, y = corrected double integral of stoichiometric $Y_D^\bullet$ signal, z = temperature dependence factor for the Fe^{3+} signal (z = 1.53 at 3.6 K) (*17*), and the remaining constants are due to Aasa and Vänngård (*40*).

Illumination-induced EPR signals around g ≈ 2 were deconvoluted into their $Y_D^\bullet$ and Chl^+/Car^+ components by fitting with a pure $Y_D^\bullet$ signal, obtained using the above procedure, and with a pure Chl^+/Car^+ signal, obtained by the following procedure. First, a PSII sample was illuminated at 133 K to produce both $Y_D^\bullet$ and Chl^+/Car^+ EPR signals. Second, the sample was incubated in the dark at 195 K for 30 min, after which time most of the Chl^+/Car^+ signal had disappeared due to reductive charge recombination reactions, while the $Y_D^\bullet$ signal remained unchanged. The difference of the two spectra, therefore, represented a pure Chl^+/Car^+ signal.

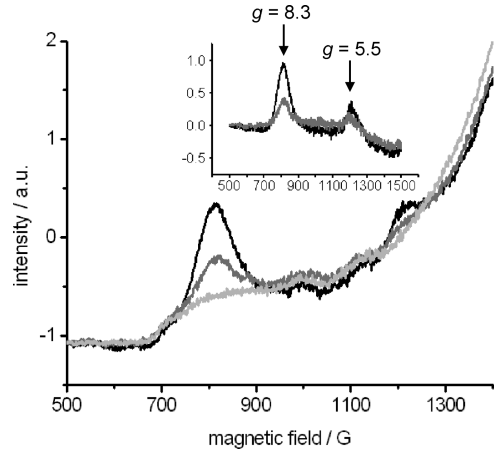

FIGURE 2: EPR spectra measured at 3.6 K showing the temperature dependence of the photoreduction of the $Fe^{3+}Q_A$ site, with exogenous glycolate coordination. Main figure: black = initial, fully oxidized non-heme iron signal; gray = signal following 5 min illumination at 3.6 K; light gray = signal following further 5 min illumination at 143 K. Inset figure: difference EPR spectra at 3.6 K of the oxidized non-heme iron of PSII. Black = black − light gray (main figure); gray = gray − light gray (main figure). EPR spectrometer conditions: microwave frequency, 9.39 GHz; microwave power, 1 mW; modulation frequency, 100 kHz; and modulation amplitude, 31 G. Spectra averaged from four scans.

RESULTS

Complete Non-Heme Iron Oxidation by Ferricyanide. Figure 2 shows the EPR peaks at g = 8.3 and g = 5.5 due to fully oxidized non-heme Fe^{3+} in PSII ligated by glycolate at pH 6.5. Integration of the g = 8.3 signal and comparison with the double integral of the $g \approx 2$ signal obtained from stoichiometric oxidation of Y_D (*17*) indicated that 100% of the iron centers were oxidized by overnight incubation with 4 mM ferricyanide and 40 mM sodium glycolate and that complete oxidation was retained after ferricyanide was

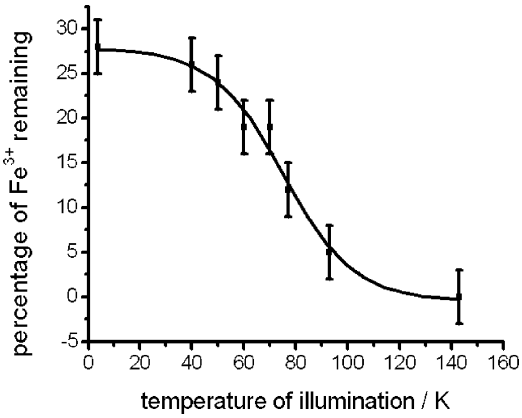

FIGURE 3: Photoreduction of the $Fe^{3+}Q_A$ site at increasing temperatures, measured with EPR spectroscopy. Illuminations of 5 min duration were found to establish equilibrium at each temperature. Sample and EPR spectrometer conditions as in Figure 2.

washed out of the sample in darkness (data not shown). Samples were found to exhibit partial non-heme iron oxidation even without the addition of ferricyanide, presumably due to oxidation by dissolved oxygen (*24*).

$Fe^{3+}Q_A$ Photoreduction. Figures 2 and 3 show the progressive photoreduction of the $Fe^{3+}Q_A$ site with increasing temperature. Five minutes of illumination at the lowest obtainable temperature (3.6 K) reproducibly abolished 70−75% of the Fe^{3+} signal, but complete abolition was only achieved at temperatures above ca. 140 K. Figure 3 shows the data fitted with a sigmoidal curve, indicating that, at 75 K, 50% of the remaining 25−30% of the Fe^{3+} signal was abolished. These data reveal that, at low temperatures, there are two distinct populations of oxidized non-heme iron centers, only one of whose EPR signal (comprising 70−75% of the total) is abolished at the lowest temperatures. This result was identical in the presence and absence of glycolate, although easier to measure in its presence because of the more complete initial oxidation of the non-heme iron.

These two populations probably represent different conformations around the metal site, which have been "frozen in" at liquid helium temperatures, preventing interconversion. The likely nature of these populations will be discussed below.

Photooxidation of Chlorophylls, Carotenoids, Y_D, and Y_Z at 30 K. At liquid helium temperatures, photoreduction of the $Fe^{3+}Q_A$ site is accompanied by the photooxidation of redox-active chlorophylls and carotenoids, as well as Y_D and Y_Z. Cytochrome b_{559} is unavailable as an electron donor because it is preoxidized by incubation in millimolar ferricyanide. Y_D is partially preoxidized under the conditions of our sample preparation, and its further oxidation is somewhat suppressed by the use of pH values below 7.0, although not completely, as in the case of Mn-depleted spinach PSII (*39*). $Y_Z^\bullet$ signals, which appear in the same region as the Y_D signal, were prevented from making a significant contribution to the spectra by the use of low, 3 μW microwave power (the $Y_Z^\bullet$ signal is typically obtained at 100 mW power (*1*)). The rapid cryogenic decay of $Y_Z^\bullet$ radicals (*41*) allowed the $Y_Z^\bullet$ contribution to be further minimized by obtaining the first spectrum several minutes after illumination had ceased.

Figure 4 shows the rise in the sharp $g \approx 2$ EPR signal, mostly attributable to oxidized chlorophyll and carotenoid cation radicals, upon illumination at 30 K. The solid lines

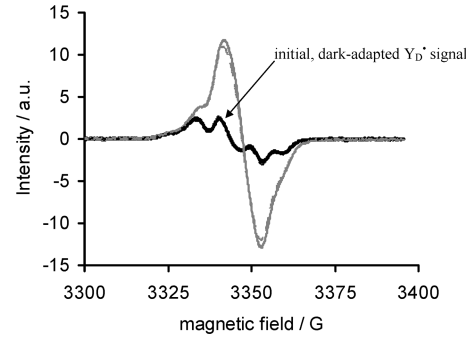

FIGURE 4: EPR spectra obtained at 30 K, showing the initial $Y_D^\bullet$ EPR signal (black line) and the increase in Chl^+, Car^+, and $Y_D^\bullet$ yields after illumination (gray lines) at 30 K which does not depend on the initial population of oxidized non-heme Fe^{3+}. Solid lines show photooxidation with an original non-heme Fe^{3+} population of 100%, whose Fe^{3+} signal was reduced to 30% of the total centers by illumination (see Figure 3). Dashed lines show photooxidation with an original non-heme Fe^{3+} population of 20%, whose Fe^{3+} signal was reduced to 5% of the total centers by illumination. The initial Fe^{3+} population of 20% was achieved by illumination for 4 min at 198 K (abolishing the Fe^{3+} signal; see Figure 3) followed by 1 min dark incubation at 273 K. EPR spectrometer conditions: microwave frequency, 9.38 GHz; microwave power, 3 μW; modulation frequency, 100 kHz; and modulation amplitude, 2 G.

show the photooxidation produced upon illumination when the non-heme iron was initially fully preoxidized (case 1), and the dashed lines show the photooxidation produced when only 20% of the non-heme iron centers were preoxidized (case 2). (20% oxidation represents the minimum attainable yield of Fe^{3+}, produced by air oxidation of the glycolate-substituted non-heme iron center, without adding an exogenous reductant.) In both illuminations, ca. 70% of the Fe^{3+} signal originally present was abolished (see Figure 3), equal to 70% of the total $Fe^{3+}Q_A$ centers in case 1 and 15% of the total centers in case 2. With initially fully oxidized non-heme iron (solid lines), deconvolution showed that chlorophyll and carotenoid radicals increased from 0 to 0.98 oxidized centers/reaction center, while the $Y_D^\bullet$ population increased from 0.60 to 0.80 per reaction center. In the second case (dashed lines), with much less non-heme iron preoxidized, chlorophyll and carotenoid radicals increased from 0.03 to 0.92 oxidized centers/reaction center, while the $Y_D^\bullet$ population increased from 0.64 to 0.80/reaction center. In other words, the yields of Chl^+, Car^+, and $Y_D^\bullet$ upon illumination were essentially identical, regardless of whether 100% (case 1) or 20% (case 2) of the non-heme iron was initially oxidized and therefore available as an electron acceptor.

We note that the calculated yields of photooxidized products in both cases slightly exceeded 100% (118% and 105% in cases 1 and 2, respectively), but this result was not always obtained, and it is likely that a small error in quantification is to blame: the procedure used to produce stoichiometric oxidation of $Y_D^\bullet$ in fact probably produced a slightly substoichiometric oxidation, leading to an overestimation of the yields of the other donors. Within error, therefore, we consistently obtained a full, single charge separation in both cases, a conclusion supported by examination of the $Fe^{2+}Q_A^-$ EPR signals (see below).

Figure 5 shows the decline of the $Y_D^\bullet$ and Chl^+/Car^+ radical EPR signals by charge recombination following their photochemical generation at 30 K, first after equilibration

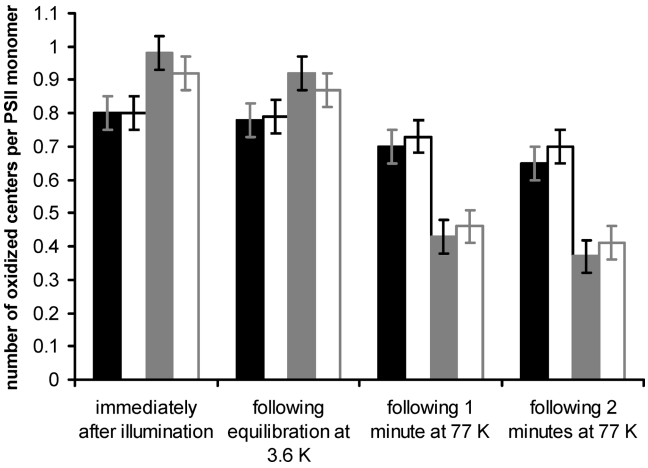

FIGURE 5: Bar chart showing the decay of $Y_D^{\bullet}$ (black outlined bars) and Chl^+/Car^+ radicals (gray outlined bars) following initial illumination at 30 K. Two cases are illustrated (see text), one in which the non-heme iron was 100% preoxidized (filled bars) and one in which the non-heme iron was only 20% preoxidized (unfilled bars). Sample and EPR spectrometer conditions as in Figure 4.

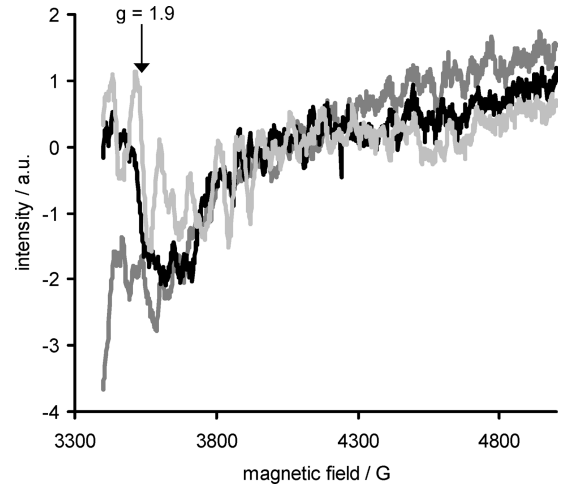

FIGURE 6: EPR difference spectra (illuminated − dark-adapted) at 6.0 K showing the $Fe^{2+}Q_A^-$ signal at $g = 1.9$ following a 30 K illumination of a PSII membrane sample in which 100% (gray) and 20% (black) of the non-heme iron was preoxidized, and following a 143 K illumination in which 100% of the non-heme iron was preoxidized (light gray). EPR spectrometer conditions: microwave frequency, 9.39 GHz; microwave power, 5 mW; modulation frequency, 100 kHz; and modulation amplitude, 31 G.

at 3.6 K (second group of columns), then after incubation in darkness for 1 min at 77 K (third group), and finally after a further 1 min of incubation in darkness at 77 K (fourth group). The decline of the $Y_D^{\bullet}$ and Chl^+/Car^+ signals was the same (within error) regardless of whether 100% or 20% of charge separations involved the reduction of the $Fe^{3+}Q_A$ center, showing that the charge separations involving the reduction of this center were no more stable than those involving the reduction of $Fe^{2+}Q_A$ to produce $Fe^{2+}Q_A^-$.

Measurement of the $Fe^{2+}Q_A^-$ EPR Signal. In order to confirm that the fully oxidized $Fe^{3+}Q_A$ site was not doubly reduced by photoreduction at 30 K, we looked for the EPR signal due to the fully reduced $Fe^{2+}Q_A^-$ center. As it was impossible to observe the small $Fe^{2+}Q_A^-$signal in the presence of high concentrations of ferricyanide, experiments were performed on samples in which ferricyanide had been washed out while leaving 100% of the non-heme iron centers oxidized. In contradiction to a previous report (*24*), it was found that a $g = 1.9$ $Fe^{2+}Q_A^-$ signal (*42*) was observed upon illumination when the non-heme iron was coordinated by glycolate (see Figure 6). No $Fe^{2+}Q_A^-$ signal was observed in experiments in which the non-heme iron was initially fully preoxidized and $Fe^{3+}Q_A$ acted as the only electron acceptor (gray line in Figure 6). In contrast, a significant $Fe^{2+}Q_A^-$ signal was seen when the non-heme iron was only partially preoxidized and $Fe^{2+}Q_A$ (one-electron-reduced iron-quinone site) acted as the majority electron acceptor (black line in Figure 6). (A correlation has previously been found between the extent of non-heme iron oxidation and the size of the $Fe^{2+}Q_A^-$ $g = 1.9$ EPR signal (*43*).) These results are consistent with the hypothesis that there was little or no double reduction of the $Fe^{3+}Q_A$ species to produce $Fe^{2+}Q_A^-$ upon illumination at 30 K. After illumination of a sample initially containing 100% $Fe^{3+}Q_A$, we conclude that approximately 70% of the centers contained a one-electron-reduced iron-quinone center which yielded no Fe^{3+} signal, and approximately 30% contained a one-electron-reduced iron-quinone center which yielded a Fe^{3+} signal. After illumination of a sample initially containing 20% $Fe^{3+}Q_A$ and 80% $Fe^{2+}Q_A$, we conclude that approximately 80% of centers contained the fully reduced $Fe^{2+}Q_A^-$ species, 15% contained the one-electron-reduced iron-quinone center yielding no Fe^{3+} signal, and 5% contained the one-electron-reduced iron-quinone center yielding a Fe^{3+} signal.

When PSII with fully oxidized non-heme iron was illuminated at the higher temperature of 143 K, all of the non-heme Fe^{3+} was photoreduced (see Figure 3), but the yield of Chl^+/Car^+ was lower than it was following illumination at 30 K because of rapid decay reactions of these unstable cation radicals. A significant $Fe^{2+}Q_A^-$ signal was observed (light gray line in Figure 6), indicating that a high proportion of double charge separations occurred under these conditions. At these temperatures the oxygen-evolving complex becomes an effective electron donor, as the S_1 to S_2 transition of the OEC is allowed to occur (*44*).

Recombination ET Reactions Leading to Oxidation of the Non-Heme Iron. In PSII whose non-heme iron had been fully preoxidized, illumination at 30 K led to the production of one $Car^+/Car^+/Y_D^{\bullet}$ radical per PSII. Upon warming from 30 K in the absence of ferricyanide, recombination of the charge separations was observed, leading to reduction of Chl^+/Car^+ and $Y_D^{\bullet}$ and partial oxidation of the iron-quinone center. As Figure 7 shows, the Fe^{3+} EPR signal did not rise to its original intensity representing 1 Fe^{3+}/PSII monomer. Gradual warming in the dark to 273 K caused the $g = 8.3$ signal to increase from 27% of total centers (immediately following illumination, marked as "start" in Figure 7) to 44% of total centers, while the Chl^+/Car^+ signal diminished to zero, and the $Y_D^{\bullet}$ signal returned to a little below its original dark-stable value.

The 30 K illumination used in the experiment described in Figure 7 yielded oxidized centers (Chl^+, Car^+, $Y_D^{\bullet}$) in 96% of PSII complexes, meaning that essentially all of the PSII complexes underwent charge separation; 73% of the PSII complexes contained an iron-quinone site after the 30 K illumination which did not exhibit a $g = 8.3/5.5$ non-heme Fe^{3+} EPR signal, while 27% contained an iron-quinone site which did exhibit a $g = 8.3/5.5$ non-heme Fe^{3+} EPR

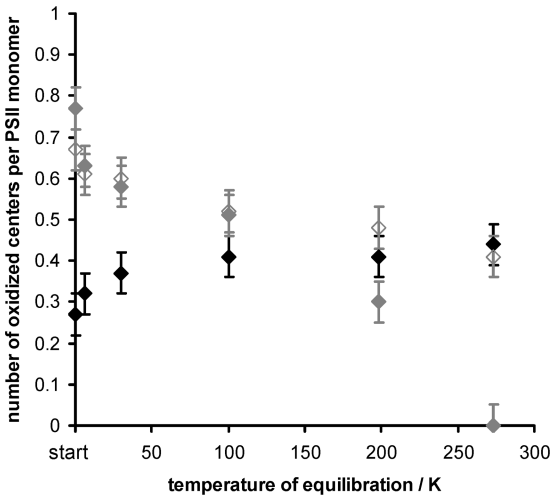

FIGURE 7: Temperature dependence of dark decay of photogenerated Chl^+/Car^+ (solid gray diamods) and $Y_D^\bullet$ (open gray diamonds) and accompanying increase in the non-heme Fe^{3+} (solid black diamonds). The values indicated at "start" are those immediately following illumination at 30 K. One hour was allowed for equilibration at each temperature, while purging with He(g) at the three highest temperatures. The original, dark-adapted populations were as follows: non-heme $Fe^{3+} = 100\%$; $Y_D^\bullet = 48\%$; $Chl^+/Car^+ = 0\%$.

signal. By the end of the gradual warming process depicted in Figure 7, after equilibration at 273 K, all of the photogenerated chlorophyll and carotenoid cation radicals had been reduced (77% of total centers) and in 26% of centers $Y_D^\bullet$ had been reduced, meaning that almost exactly 100% of the photooxidized centers were observed to reductively decay. This reductive decay must have been accompanied by oxidation of one species per PSII monomer. However, as Figure 7 shows, the increase of the non-heme Fe^{3+} $g = 8.3$ signal accounts for only 17% of centers (an increase from 27% to 44% of centers). The rest of the charge separations, representing 60% of the PSII centers, underwent reduction of the oxidized species without any apparent corresponding oxidation of the non-heme iron. This curious mismatch is discussed below.

DISCUSSION

This work has focused on the characterization of non-heme Fe^{3+} photoreduction and recombination reactions. It is important to distinguish between the present work, in which the non-heme Fe^{3+} has been used as an electron acceptor at very low temperatures, and previous work in which the non-heme Fe^{3+} was used as an electron acceptor at temperatures up to 243 K (*14*). In contrast to these previous studies, in which double turnover of the OEC was observed ($S_1 \rightarrow S_2 \rightarrow S_3$), no double charge separation was seen in PSII centers in the present work after illumination at 30 K or below. The higher temperatures required for the simultaneous reduction of Q_A and the non-heme Fe^{3+} are inimical to the establishment of high yields of oxidized chlorophylls and carotenoids, which are rapidly reduced by charge recombination above liquid helium temperatures (*4*).

We observed that 70−75% of the $Fe^{3+}Q_A$ centers were photoreduced even at the lowest temperatures (ca. 4 K) to an EPR-inactive state, abolishing the $g = 8.3$ and $g = 5.5$ signals due to these centers. In contrast, the signals due to the remaining 25−30% of the $Fe^{3+}Q_A$ centers were only fully

Scheme 1: Cryogenic Redox Interconversions of the Iron-Quinone Site in Conformations A (Ovals) and B (Rectangles)[a]

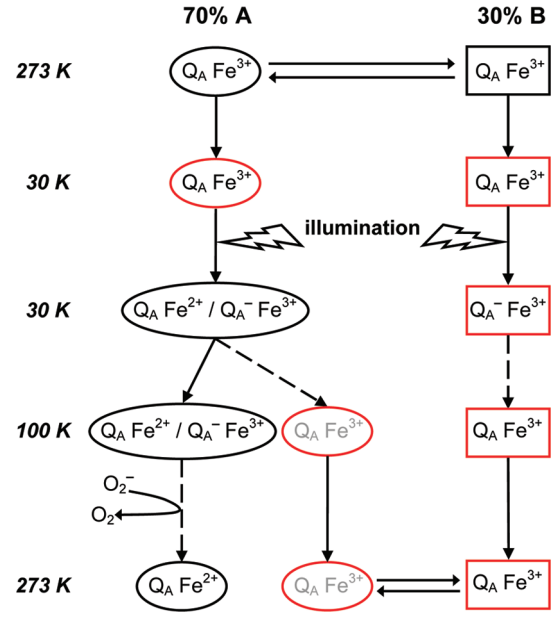

[a] Iron-quinone sites yielding $g = 8.3$ and $g = 5.5$ EPR signals are colored red. Recombination reactions involving the reduction of Chl^+, Car^+, and $Y_D^\bullet$ are indicated by dashed arrows. Minor species are indicated by gray lettering.

abolished by illumination at much higher temperatures (above ca. 140 K), with a half-reduction temperature of 75 K.

This difference in behavior between the two populations is presumably the result of differences in protein structure around the non-heme iron site. Renger and co-workers have measured the temperature-dependent dynamics of the PSII non-heme iron site with Mössbauer spectroscopy and found that large-amplitude motions in this part of the protein are absent below 230 K (*45*). The same group has recently investigated the overall dynamics of PSII using quasielastic neutron scattering and found a similar transition temperature of 240 K for large-amplitude motions, as well as an onset temperature of 120 K for restricted protein movement (*46*) which was not observed in the non-heme site (*45*). We conclude that the half-reduction temperature of 75 K observed in our work does not correspond to the onset of either large-amplitude or restricted protein movements that are able to interconvert the two iron-quinone structural populations. We hypothesize instead that there are two distinct non-heme iron structural environments (or groups of environments) that are "frozen in" below ca. 140 K. The non-heme iron EPR signal in environment A may be fully abolished by illumination at all temperatures, while the signal due to iron in environment B may be abolished by illumination only at temperatures above 75 K. These two structures may well be similar to the two microenvironments of the reduced non-heme iron site observed at 80 K in an earlier Mössbauer spectroscopy study (*47*).

There are two ways of viewing the redox reactions of populations A and B, as described in Scheme 1. The most straightforward interpretation of the data is to assume that abolition of the $g = 8.3$ and $g = 5.5$ EPR signals indicates the reduction of Fe^{3+} to Fe^{2+}. This interpretation would imply

that, after a 30 K illumination of a PSII sample in which all of the non-heme iron was initially preoxidized, 70−75% of the sample would be in the $Fe^{2+}Q_A$ (EPR-inactive) state and 25−30% in the $Fe^{3+}Q_A^-$ (EPR-active) state. The latter state appears to exhibit some magnetic interaction between Fe^{3+} and Q_A^-: weak enough for the broad $g = 8.3$ Fe^{3+} signal not to be further broadened upon photoreduction of the iron-quinone site (see Figure 2, inset) but strong enough for the Q_A^- signal to be broadened so that it does not contribute significantly to the sharp $g = 2$ radical signals (see Figure 4) Indeed, the fact that these $g = 2$ signals cross the baseline at the same point regardless of the original Fe^{3+} content rules out any significant influence of the iron's oxidation state on the amount of uncoupled Q_A^- after illumination at 30 K, since the semiquinone's higher *g*-value would shift the baseline crossing to lower field.

In an alternative interpretation, the majority of the non-heme iron EPR signals are abolished not by reduction of the iron itself but by reduction of the neighboring Q_A to Q_A^-. A strong magnetic interaction between Fe^{3+} and Q_A^- might be enough to split the Fe^{3+} EPR signal into several weak, unobserved components. In this interpretation, after a 30 K illumination of a PSII sample in which all of the non-heme iron was initially preoxidized, 70−75% of the sample would be in the strongly interacting $Fe^{3+}Q_A^-$ (EPR-inactive) state and 25−30% in a $Fe^{3+}Q_A^-$ (EPR-active) state in which Fe^{3+} and Q_A^- do not magnetically interact.

Our data do not allow us to distinguish between these two alternatives, although possibly Mössbauer or UV spectroscopy could be used. Whether the electron resides on Fe^{2+} or on Q_A^- in environment A after illumination at 4−30 K, illumination at higher temperatures does reduce the non-heme iron, since a substantial $Fe^{2+}Q_A^-$ signal was seen after illumination at 143 K (see Figure 6.) On the basis of this observation, together with the evidence against a conformational change at the iron-quinone site below 230 K discussed above, we conclude that the loss of the $g = 8.3/5.5$ Fe^{3+} EPR in conformation B by illumination at temperatures above ca. 75 K (Figure 3) is due to Fe^{3+} reduction by Q_A^-. It is likely that reduction of the non-heme iron is achieved by proton-coupled electron transfer (PCET) at pH 6.5 and that proton transfer within the protein to the vicinity of the non-heme iron is rate-limiting for reduction of the non-heme iron at cryogenic temperatures. From this, it follows that a proton is able to move within the protein to the vicinity of the non-heme iron at low temperatures: possibly at liquid helium temperatures in the case of environment A and most likely at temperatures above 75 K. A plausible entry point for protons near the PSII non-heme iron is the surface-exposed residue D1-E244, whose pK_a was found in a recent computational study to be sensitive to the redox state of the iron ion, being 7.5 in the presence of Fe^{2+} and 5.5 in the presence of Fe^{3+} (*25*).

Proton transfer at such low temperatures may be rationalized in terms of the environmentally coupled tunneling model of proton transfer in proteins, in which the quantum mechanical tunneling of protons is modulated by (classically treated) protein dynamics (*48*). A Marcus-type model may be used to describe this dynamic modulation, invoking an environmental reorganization energy for proton transfer that is exactly analogous to the more familiar λ for electron transfer. The activationless proton transfer possibly observed in the reduction of Fe^{3+} in population A below 30 K corresponds, in this model, to a perfectly preorganized environment for proton transfer within the protein to the non-heme iron environment. The proton transfer reorganization energy, in other words, is exactly matched to the driving force of the reaction, a configuration which has been described as "tunneling-ready" (*49*). In contrast, environment B is not perfectly preorganized for proton transfer during reduction, exhibiting a proton-transfer reorganization energy and consequently displaying a nonzero activation energy of 75 K × R = 0.6 kJ mol^{-1}. The environmentally coupled tunneling model has previously been used to rationalize proton transfers at cryogenic temperatures to the active sites of heme oxygenase and cytochrome P450 (*50*). Interestingly, rapid proton transfer to the active site of heme oxygenase occurs at 4.2 K over a straight-line distance of ca. 17 Å, while in PSII the distance between the non-heme iron and D1-E244 is only ca. 8 Å (*19*).

The existence of a low reorganization energy proton-transfer pathway to the vicinity of the non-heme iron provides circumstantial evidence that such a transfer is physiologically important, as it is in heme oxygenase and cytochrome P450. There are two ways in which this might be the case. The first is in the catalytic situation, in which the non-heme iron apparently remains in the reduced state as electrons pass from Q_A^- to Q_B (*51*). It is the PCET reactions of Q_B that are relevant to the donor-side main-chain electron transfer, because Q_B accepts two protons along with two electrons to form the quinol QH_2. The means by which Q_B obtains protons from bulk is unknown, although two pathways have been suggested: one involves D1-S264 and D1-H252 (*52*) and the other the iron-bound bicarbonate (*53*). Such a pathway, involving D1-E244, bicarbonate, and D1-H215, is recommended both by a favorable pK_a gradient (glutamate p$K_a \approx 4$, bicarbonate p$K_a \approx 6$, histidine p$K_a \approx 6$, Q_B^- p$K_a \approx 8$) and by the explanation it would provide for the influence of bicarbonate on acceptor-side electron transfer (*54*). Although in the current work we have substituted glycolate (p$K_a \approx 4$) for bicarbonate, allowing us to begin our experiments with the non-heme iron fully oxidized, our results suggest that this proton-transfer pathway is largely or fully preorganized as far as the non-heme iron and that it may play a role in delivering protons to Q_B.

The second way in which nature might use this proton-transfer pathway is in facilitating the redox chemistry of the non-heme iron itself. It is likely that the rise in the non-heme Fe^{3+} EPR signal on warming in the dark after illumination at 30 K (see Figure 7) is due to the partial recombinative oxidation of the ferrous non-heme iron by Chl^+/Car^+ and/or $Y_D^\bullet$. Indeed, a recent report has employed this interpretation, noting the similarity of the kinetics of partial Fe^{3+} recovery with those of Chl^+/Car^+ reduction (*55*). Such an oxidation of the non-heme iron may be used by PSII centers vulnerable to photodamage in the photoprotective transfer of oxidizing power away from P_{680} and the manganese cluster. The most recent PSII crystal structure (*19*) shows that Y_D is approximately 38 Å away from the non-heme iron, too long a distance for direct electron transfer at an appreciable rate. There are several chlorophylls, however, within 25 Å of the non-heme iron that might be active in secondary electron transfer. On the CP47 side of the reaction center there is Chl*a*17 (also within 25 Å of Y_D)

and Chl*a*24, and on the CP43-side there is Chl*a*44. Some or all of these cofactors might be involved in the recombination of the $Chl^+/Car^+/Y_D^{\bullet}\cdots Fe^{2+}$ charge separation to form $Chl/Car/Y_D\cdots Fe^{3+}$.

As noted above, there is a discrepancy between the small number of non-heme iron centers apparently oxidized in these recombinations and the large number of $Chl^+/Car^+/Y_D^{\bullet}$ centers reduced. As the temperature was increased to around 100 K in the dark, Figure 7 shows that the Fe^{3+} signal reappears in 14% of the PSII centers, and the oxidized Chl^+, Car^+, and $Y_D^{\bullet}$ signals disappear in 41% of the centers. We believe it is likely that all of the 27% of PSII centers that retained the Fe^{3+} signal upon charge separation at 30 K (weakly coupled $Fe^{3+}Q_A^-$ centers in conformation B) recombine in this temperature range, along with 14% of centers in conformation A that had lost the Fe^{3+} signal upon illumination (either through non-heme Fe^{3+} or Q_A reduction). As the temperature was increased above 100 K in the dark, the Fe^{3+} signal hardly grows at all, while the Chl^+, Car^+, and $Y_D^{\bullet}$ signals disappear in 62% of the centers (overall these species were reduced in 103% of centers, corresponding to all of the PSII within error). These observations cannot be explained by charge recombination between the iron-quinone site and Chl^+, Car^+, and $Y_D^{\bullet}$. If the original 30 K illumination produced strongly coupled $Fe^{3+}Q_A^-$ rather than $Fe^{2+}Q_A$ in the majority of centers, it is possible that Fe^{3+} is reduced by Q_A^- at higher temperatures, giving $Fe^{2+}Q_A$ on the acceptor side. However, this still leaves open the question of what reduces the remaining Chl^+, Car^+, and $Y_D^{\bullet}$ centers. It may be that, at temperatures above 140 K, these high-potential species oxidize the OEC more rapidly than they do the non-heme iron, although no S_2 multiline signal was seen under the experimental conditions used. Alternatively, it is possible that the non-heme iron is indeed recombinatively oxidized but that it is immediately exogenously rereduced. One candidate for the reducing agent is a local concentration of superoxide, known to be produced at the acceptor side of PSII (*56*). A value for $E°(Fe^{3+/2+}(A))$ of $\geq +370$ mV would mean that superoxide, with a "dissolved" reduction potential (relative to 1 M O_2) of $E(O_2(aq)/O_2^-)$ of -160 mV (*57*), would prove a rapid reductant of this population of the non-heme iron (approximately on the millisecond time scale).

It is interesting to note that recombinative oxidation of the ferrous non-heme iron by Chl^+/Car^+ and/or $Y_D^{\bullet}$ was not observed in previous work in which Q_A alone was used as a cryogenic electron acceptor (*4*). It is likely that the non-heme Fe^{2+} was entirely frozen into a high-reduction-potential conformation in this previous work and was, therefore, unable to reduce the secondary electron donors. Recent spectroscopic studies on Q_B in the bacterial reaction center suggest a structural basis for this difference in redox behavior (*58*). Paddock and co-workers found that the "relaxed" hydrogen-bonding environment of Q_B in reaction centers that are frozen to 77 K under illumination differs from the "unrelaxed" environment seen around Q_B in reaction centers illuminated only at 77 K. In the relaxed environment, a hydrogen-bonded proton-transfer pathway exists between the protein surface and Q_B, a difference that is partially responsible for the much greater charge recombination rates displayed by the relaxed quinone. We propose that an analogous difference in the hydrogen-bonding environment of the non-heme iron explains our observation that only iron centers that are originally frozen in the oxidized state are able to be recombinatively oxidized by secondary electron donors. We note, too, that our previous work (*4*) was carried out in ethylene glycol cryoprotectant, under which conditions we have never observed significant oxidation of the PSII non-heme iron.

SUMMARY AND CONCLUSIONS

We have characterized the cryogenic temperature dependence of the photoreduction of PSII's preoxidized non-heme iron. The $Fe^{3+}Q_A$ site adopted two structures below 75 K and acted as a single electron-accepting moiety. In both populations, a full, single charge separation was established between various secondary electron donors (Chl^+, Car^+, $Y_D^{\bullet}$) and the iron-quinone site. The two populations displayed the same stabilities with respect to recombination at higher temperatures as did the Chl^+, Car^+, $Y_D^{\bullet}\cdots Fe^{2+}Q_A^-$ charge separation. Cryogenic photoreduction of the non-heme iron site (possibly at liquid helium temperatures and certainly above 75 K) indicates that the surrounding protein structure is organized for fast proton transfer within the protein to the iron-quinone site. This may be physiologically relevant in the catalytic PCET reactions of Q_B and/or in a possible photoprotective role of the non-heme iron itself. Evidence for such a role comes from our observation of partial oxidation by secondary electron donors (Chl^+, Car^+, $Y_D^{\bullet}$) of the non-heme iron and its rapid exogenous reduction.

ACKNOWLEDGMENT

We thank the anonymous reviewers for helpful comments.

REFERENCES

1. Zhang, C. X., and Styring, S. (2003) Formation of split electron paramagnetic resonance signals in photosystem II suggests that tyrosine Z can be photooxidized at 5 K in the S_0 and S_{-1} states of the oxygen-evolving complex. *Biochemistry 42*, 8066–8076.
2. Diner, B. A., and Britt, R. D. (2005) The redox-active tyrosines Y_Z and Y_D, in *Photosystem II: The Light-Driven Water:Plastoquinone Oxidoreductase* (Wydrzynski, T. J., and Satoh, K., Eds.) pp 207−233, Springer, Dordrecht.
3. Stewart, D. H., and Brudvig, G. W. (1998) Cytochrome b_{559} of photosystem II. *Biochim. Biophys. Acta 1367*, 63–87.
4. Tracewell, C. A., Cua, A., Stewart, D. H., Bocian, D. F., and Brudvig, G. W. (2001) Characterization of carotenoid and chlorophyll photooxidation in photosystem II. *Biochemistry 40*, 193–203.
5. Kitajima, Y., and Noguchi, T. (2006) Photooxidation pathway of chlorophyll Z in photosystem II as studied by Fourier transform infrared spectroscopy. *Biochemistry 45*, 1938–1945.
6. Hanley, J., Deligiannakis, Y., Pascal, A., Faller, P., and Rutherford, A. W. (1999) Carotenoid oxidation in photosystem II. *Biochemistry 38*, 8189–8195.
7. Frank, H. A., and Brudvig, G. W. (2004) Redox functions of carotenoids in photosynthesis. *Biochemistry 43*, 8607–8615.
8. Nugent, J. H. A., Diner, B. A., and Evans, M. C. W. (1981) Direct detection of the electron acceptor of photosystem II. *FEBS Lett. 124*, 241–244.
9. Petrouleas, V., and Diner, B. A. (1986) Identification of Q_{400}, a high-potential electron-acceptor of photosystem II, with the iron of the quinone-iron acceptor complex. *Biochim. Biophys. Acta 849*, 264–275.
10. Ikegami, I., and Katoh, S. (1973) Studies on chlorophyll fluorescence in chloroplasts II. Effects of ferricyanide on the induction of fluorescence in the presence of 3-(3,4-dichlorophenyl)-1,1-dimethylurea. *Plant Cell Physiol. 14*, 829–836.
11. Mamedov, M. D., Tyunyatkina, A. A., Siletsky, S. A., and Semenov, A. Y. (2006) Voltage changes involving photosystem II quinone-iron complex turnover. *Eur. Biophys. J. 35*, 647–654.

12. Wraight, C. A. (1985) Modulation of herbicide binding by the redox state of Q_{400}, an endogenous component of photosystem II. *Biochim. Biophys. Acta 809*, 320–330.
13. Diner, B. A., and Petrouleas, V. (1987) Q_{400}, the non-heme iron of the photosystem II iron-quinone complex—a spectroscopic probe of quinone and inhibitor binding to the reaction center. *Biochim. Biophys. Acta 895*, 107–125.
14. Guiles, R. D., Zimmermann, J. L., McDermott, A. E., Yachandra, V. K., Cole, J. L., Dexheimer, S. L., Britt, R. D., Wieghardt, K., Bossek, U., Sauer, K., and Klein, M. L. (1990) The S_3 state of photosystem II: Differences between the structure of the manganese complex in the S_2 and S_3 states determined by X-ray absorption spectroscopy. *Biochemistry 29*, 471–485.
15. Ioannidis, N., and Petrouleas, V. (2000) Electron paramagnetic resonance signals from the S_3 state of the oxygen-evolving complex. A broadened radical signal induced by low-temperature near-infrared light illumination. *Biochemistry 39*, 5246–5254.
16. Nugent, J. H. A., Turconi, S., and Evans, M. C. W. (1997) EPR investigation of water oxidizing photosystem II: Detection of new EPR signals at cryogenic temperatures. *Biochemistry 36*, 7086–7096.
17. Aasa, R., Andréasson, L. E., Styring, S., and Vänngård, T. (1989) The nature of the Fe(III) EPR signal from the acceptor-side iron in photosystem II. *FEBS Lett. 243*, 156–160.
18. Ferreira, K. N., Iverson, T. M., Maghlaoui, K., Barber, J., and Iwata, S. (2004) Architecture of the photosynthetic oxygen-evolving center. *Science 303*, 1831–1838.
19. Loll, B., Kern, J., Saenger, W., Zouni, A., and Biesiadka, J. (2005) Towards complete cofactor arrangement in the 3.0 Å resolution structure of photosystem II. *Nature 438*, 1040–1044.
20. Michel, H., and Deisenhofer, J. (1988) Relevance of the photosynthetic reaction center from purple bacteria to the structure of photosystem II. *Biochemistry 27*, 1–7.
21. Diner, B. A., and Petrouleas, V. (1990) Formation by NO of nitrosyl adducts of redox components of the photosystem II reaction center. 2. Evidence that HCO_3^-/CO_2 binds to the acceptor-side non-heme iron. *Biochim. Biophys. Acta 1015*, 141–149.
22. Hienerwadel, R., and Berthomieu, C. (1995) Bicarbonate binding to the non-heme iron of photosystem II investigated by Fourier transform infrared difference spectroscopy and ^{13}C-labeled bicarbonate. *Biochemistry 34*, 16288–16297.
23. Petrouleas, V., Deligiannakis, Y., and Diner, B. A. (1994) Binding of carboxylate anions at the non-heme Fe(II) of PSII. 2. Competition with bicarbonate and effects on the Q_A/Q_B electron transfer rate. *Biochim. Biophys. Acta 1188*, 271–277.
24. Deligiannakis, Y., Petrouleas, V., and Diner, B. A. (1994) Binding of carboxylate anions at the non-heme Fe(II) of PSII. 1. Effects on the $Q_A^-Fe^{2+}$ and Q_AFe^{3+} EPR spectra and the redox properties of the iron. *Biochim. Biophys. Acta 1188*, 260–270.
25. Ishikita, H., and Knapp, E. W. (2005) Oxidation of the non-heme iron complex in photosystem II. *Biochemistry 44*, 14772–14783.
26. Kurreck, J., Garbers, A., Reifarth, F., Andréasson, L. E., Parak, F., and Renger, G. (1996) Isolation and properties of PS II membrane fragments depleted of the non heme iron center. *FEBS Lett. 381*, 53–57.
27. Noguchi, T., Kurreck, J., Inoue, T., and Renger, G. (1999) Comparative FTIR analysis of the microenvironment of Q_A^- in cyanide-treated, high pH-treated and iron-depleted photosystem II membrane fragments. *Biochemistry 38*, 4846–4852.
28. Renger, G., Kurreck, J., Haag, E., Reifarth, F., Bergmann, A., Parak, F., Garbers, A., MacMillan, F., Lendzian, F., and Lubitz, W. (1997) The non-heme iron centre of photosystem II and modulatory effects of exogenous copper (II), in *Bioinorganic Chemistry: Transition Metals in Biology and their Coordination Chemistry* (Trautwein, A. X., Ed.) pp 260−277, Wiley-VCH, Weinheim.
29. Vermaas, W., Vass, I., Eggers, B., and Styring, S. (1994) Mutation of a putative ligand to the non-heme iron in photosystem II: Implications for Q_A reactivity, electron transfer, and herbicide binding. *Biochim. Biophys. Acta 1184*, 263–272.
30. Goussias, C., Deligiannakis, Y., Sanakis, Y., Ioannidis, N., and Petrouleas, V. (2002) Probing subtle coordination changes in the iron-quinone complex of photosystem II during charge separation, by the use of NO. *Biochemistry 41*, 15212–15223.
31. van Rensen, J. J. S., Tonk, W. J. M., and de Bruijn, S. M. (1988) Involvement of bicarbonate in the protonation of the secondary quinone electron acceptor of photosystem II via the non-haem iron of the quinone-iron acceptor complex. *FEBS Lett. 226*, 347–351.
32. Koulougliotis, D., Kostopoulos, T., Petrouleas, V., and Diner, B. A. (1993) Evidence for CN^- binding at the PSII non-heme Fe^{2+}. Effects on the EPR signal for $Q_A^-Fe^{2+}$ and on Q_A/Q_B electron transfer. *Biochim. Biophys. Acta 1141*, 275–282.
33. Sheptovitsky, Y. G., and Brudvig, G. W. (1998) Catalase-free photosystem II: The O_2-evolving complex does not dismutate hydrogen peroxide. *Biochemistry 37*, 5052–5059.
34. Pospisil, P., Arato, A., Krieger-Liszkay, A., and Rutherford, A. W. (2004) Hydroxyl radical generation by photosystem II. *Biochemistry 43*, 6783–6792.
35. McEvoy, J. P., and Brudvig, G. W. (2008) Redox reactions of the non-heme iron of photosystem II: An EPR spectroscopic study, in *Photosynthesis: Energy from the Sun* (Allen, J. F., Gantt, E., Golbeck, J. H., and Osmond, B., Eds.) pp 141−144, Springer, Dordrecht.
36. Berthold, D. A., Babcock, G. T., and Yocum, C. F. (1981) A highly resolved, oxygen-evolving photosystem II preparation from spinach thylakoid membranes: Electron paramagnetic resonance and electron transport properties. *FEBS Lett. 134*, 231–234.
37. Arnon, D. I. (1949) Copper enzymes in isolated chloroplasts: polyphenoloxidase in *Beta vulgaris*. *Plant Physiol. 24*, 1–15.
38. Boussac, A., Un, S., Horner, O., and Rutherford, A. W. (1998) High-spin states ($S > 5/2$) of the photosystem II manganese complex. *Biochemistry 37*, 4001–4007.
39. Faller, P., Rutherford, A. W., and Debus, R. J. (2002) Tyrosine D oxidation at cryogenic temperature in photosystem II. *Biochemistry 41*, 12914–12920.
40. Aasa, R., and Vänngård, T. (1975) EPR signal intensity and powder shapes: a re-examination. *J. Magn. Reson. 19*, 308–315.
41. Ioannidis, N., Zahariou, G., and Petrouleas, V. (2008) The EPR spectrum of tyrosine $Z^\bullet$ and its decay kinetics in O_2-evolving photosystem II preparations. *Biochemistry 47*, 6292–6300.
42. Rutherford, A. W., and Zimmermann, J. L. (1984) A new EPR signal attributed to the primary plastosemiquinone reaction center in photosystem II. *Biochim. Biophys. Acta 767*, 168–175.
43. Petrouleas, V., and Diner, B. A. (1987) Light-induced oxidation of the acceptor-side Fe(II) of photosystem II by exogenous quinones acting through the Q_B binding site. 1. Quinones, kinetics and pH-dependence. *Biochim. Biophys. Acta 893*, 126–137.
44. Casey, J. L., and Sauer, K. (1984) Electron paramagnetic resonance detection of a cryogenically photogenerated intermediate in photosynthetic oxygen evolution. *Biochim. Biophys. Acta 767*, 21–28.
45. Garbers, A., Reifarth, F., Kurreck, J., Renger, G., and Parak, F. (1998) Correlation between protein flexibility and electron transfer from $Q_A^{-\bullet}$ to Q_B in PSII membrane fragments from spinach. *Biochemistry 37*, 11399–11404.
46. Pieper, J., Hauss, T., Buchsteiner, A., Baczynski, K., Adamiak, K., Lechner, R. E., and Renger, G. (2007) Temperature- and hydration-dependent protein dynamics in photosystem II of green plants studied by quasielastic neutron scattering. *Biochemistry 46*, 11398–11409.
47. Petrouleas, V., Sanakis, Y., Deligiannakis, Y., and Diner, B. A. (1992) in *Research in Photosynthesis* (Murata, N., Ed.) pp 119−122, Kluwer Academic Publishers, Dordrecht.
48. Hammes-Schiffer, S. (2006) Hydrogen tunneling and protein motion in enzyme reactions. *Acc. Chem. Res. 39*, 93–100.
49. Pudney, C. R., Hay, S., Sutcliffe, M. J., and Scrutton, N. S. (2006) Alpha-secondary isotope effects as probes of "tunneling-ready" configurations in enzymatic H-tunneling: Insight from environmentally coupled tunneling models. *J. Am. Chem. Soc. 128*, 14053–14058.
50. Davydov, R., Chemerisov, S., Werst, D. E., Rajh, T., Matsui, T., Ikeda-Saito, M., and Hoffman, B. M. (2004) Proton transfer at helium temperatures during dioxygen activation by heme monooxygenases. *J. Am. Chem. Soc. 126*, 15960–15961.
51. Hermes, S., Bremm, O., Garczarek, F., Derrien, V., Liebisch, P., Loja, P., Sebban, P., Gerwert, K., and Haumann, M. (2006) A time-resolved iron-specific X-ray absorption experiment yields no evidence for an Fe^{2+} to Fe^{3+} transition during Q_A^- to Q_B electron transfer in the photosynthetic reaction center. *Biochemistry 45*, 353–359.
52. Ishikita, H., and Knapp, E. W. (2005) Control of quinone redox potentials in photosystem II: Electron transfer and photoprotection. *J. Am. Chem. Soc. 127*, 14714–14720.
53. Diner, B. A., Petrouleas, V., and Wendoloski, J. J. (1991) The iron-quinone electron-acceptor complex of photosystem II. *Physiol. Plant. 81*, 423–436.
54. van Rensen, J. J. S. (2002) Role of bicarbonate at the acceptor side of Photosystem II. *Photosynth. Res. 73*, 185–192.

55. Bao, H., Zhang, C., Kawakami, K., Ren, Y., Shen, J. R., and Zhao, J. (2008) Acceptor side effects on the electron transfer at cryogenic temperatures in intact photosystem II. *Biochim. Biophys. Acta 1777*, 1109–1115.

56. Ananyev, G. M., Renger, G., Wacker, U., and Klimov, V. V. (1994) The production of superoxide radicals and the superoxide dismutase activity of photosystem II. The possible involvement of cytochrome b_{559}. *Photosynth. Res. 41*, 327–338.

57. Wood, P. M. (1987) The two redox potentials for oxygen reduction to superoxide. *Trends Biochem. Sci. 12*, 250–251.

58. Paddock, M. L., Flores, M., Isaacson, R., Chang, C., Abresch, E. C., and Okamura, M. Y. (2007) ENDOR spectroscopy reveals light induced movement of the H-bond from Ser-L223 upon forming the semiquinone ($Q_B^{-\bullet}$) in reaction centers from *Rhodobacter sphaeroides*. *Biochemistry 46*, 8234–8243.

BI8013888